2020 IEEE International Conference on Robotics and Automation (ICRA)
31 May - 31 August, 2020. Paris, France

# Dynamic Coupling as an Indicator of Gait Robustness for Underactuated Biped Robots

Martin Fevre and James P. Schmiedeler

***Abstract*— This paper employs velocity decomposition of underactuated mechanical systems to determine the degree of dynamic coupling in the gaits of a two-link biped model. The degree of coupling between controlled and uncontrolled directions quantifies the control authority the system has over its unactuated degree of freedom. This paper shows that the amount of coupling is directly correlated to gait robustness, as seen through the size of the gait's region of attraction. The analytical measure of coupling is applied in the context of trajectory optimization to generate two-link gaits that maximize or minimize coupling. Simulation studies show that gaits maximizing coupling exhibit significantly superior robustness, as measured by 1) stochastic performance on uneven terrain, 2) ability to maintain desired walking speed under non-vanishing disturbances, 3) size of the region of attraction, and 4) robustness to model uncertainties.**

## I. Introduction

Underactuated biped robots exploit the same natural dynamics of human locomotion to produce highly efficient gaits [1], [2]. Though such robots are practical for tasks requiring long autonomy, they face complex control challenges that stem from their unactuated dynamics and their limited ability to reject large external disturbances in the unactuated degrees of freedom (DoF). These practical challenges still limit the applications of efficient dynamic walkers today.

Inspired by geometric analysis and control [3], the velocity decomposition metric in [4] uses differential geometry to partition the equations of motion of an underactuated mechanical system into its controlled and uncontrolled directions. Previously applied to the task of controller design [5], the framework improved experimental disturbance rejection of a planar, five-link underactuated biped robot [6]. The decomposition provides an analytical expression for the nonlinear dynamic coupling between the directions. The practical implication is that the measure of coupling quantifies the instantaneous control authority over the unactuated DoF [7], providing insight into its ability to reject disturbances [8].

When no coupling is available, the control inputs cannot help reject external disturbances in the uncontrolled directions. Conversely, when coupling is strong, the system has increased control authority to reject such disturbances. In biped locomotion, high-bandwidth control is necessary to achieve highly dynamic motions, and waiting for the robot to move away from a dynamic singularity is not viable. Previous work, however, suggests that the relative amount of coupling in most walking motions is low for point-foot underactuated biped robots [9], [10]. Yet, no prior work has used the velocity decomposition metric and the insight gained from it to design robust bipedal gaits.

This paper 1) analyzes the correlation between inherent dynamic coupling of a gait and its associated robustness, and 2) compares the robustness of several bipedal gaits with varying amounts of coupling. Section II presents the dynamic coupling metric and applies the method to a two-link biped model. Section III employs trajectory optimization to generate gaits for the two-link biped. Section IV investigates the correlation between coupling and robustness and compares the disturbance rejection performance of several two-link gaits when dynamic coupling was maximized/minimized.

## II. Dynamic Coupling Metric

### A. General Formulation

It is a standard result that for a mechanical system subject to external forces $\mathbf{F}$ and with a Lagrangian of the form $\mathcal{L} = \mathcal{T} - \mathcal{V}$, a smooth curve $\boldsymbol{\gamma}(t)$ satisfies the Lagrange-d'Alembert principle if it satisfies

$$\nabla_{\dot{\boldsymbol{\gamma}}(t)}\dot{\boldsymbol{\gamma}}(t) = \mathbf{M}^{-1}(\mathbf{F}(t)) - grad\ \mathcal{V}\ (\boldsymbol{\gamma}(t)), \tag{1}$$

where $\nabla$ denotes the covariant derivative and $\mathbf{M}^{-1}$ is the inverse of the inertia matrix [3]. Equation (1) is often called the coordinate-invariant representation of the equations of motion. In coordinates, this may be expressed as

$$\ddot{\theta}^i + \Gamma^i_{jk}\dot{\theta}^j\dot{\theta}^k = u^a M^{ik} F^a_k - M^{ik}\frac{\partial \mathcal{V}}{\partial \theta_k}, \tag{2}$$

where superscripts on the inertia matrix indicate the components of its inverse, $F_k$ are the components of the applied torques, $\Gamma^k_{ij}$ are the Christoffel symbols, and summation over repeated indices is implied. The dynamic coupling metric is derived using differential geometry to partition the equations of motion of underactuated mechanical systems into directions aligned with the inputs, termed controlled directions, and directions orthogonal to the inputs with respect to the inertia matrix, termed uncontrolled directions. The decomposition holds for mechanical systems with several degrees of underactuation because it applies to any underactuated mechanical system described by Lagrange's equations.

First, construct an $\mathbf{M}-$orthonormal basis with the linearly independent control forces $\mathbf{F}^a\ (a = 1, ..., m)$,

$$\mathbf{Y}_a = \frac{\mathbf{M}^{-1}\mathbf{F}^a}{||\mathbf{M}^{-1}\mathbf{F}^a||^2_{\mathbf{M}}}, \tag{3}$$

This work was supported in part by the National Science Foundation under Grant IIS-1527393.

The authors are with the Department of Aerospace & Mechanical Engineering, University of Notre Dame, IN USA.

Corresponding author: mfevre@nd.edu

where $||\cdot||^2_{\mathbf{M}}$ denotes the Euclidean norm with respect to $\mathbf{M}$. The set of vector fields $\mathcal{Y} = \{\mathbf{Y}_1, ..., \mathbf{Y}_m\} \in \mathbb{R}^{n\times m}$ represents the input distribution of the system. The $\mathbf{M}$-orthonormal complement to the input distribution is $\mathcal{Y}^\perp = \{\mathbf{Y}_1^\perp, ..., \mathbf{Y}_{n-m}^\perp\} \in \mathbb{R}^{n\times(n-m)}$ and includes the remaining $n-m$ uncontrolled directions that have unit length with respect to $\mathbf{M}$ and satisfy $\langle \mathbf{Y}_b^\perp, \mathbf{Y}_a\rangle_{\mathbf{M}} = 0$, where $\langle\cdot,\cdot\rangle_{\mathbf{M}}$ denotes the inner product with respect to $\mathbf{M}$. Consequently, the $\mathbf{M}$-orthonormal frame $\{\mathcal{Y}, \mathcal{Y}^\perp\} := \{\mathbf{Y}_1, ..., \mathbf{Y}_m, \mathbf{Y}_1^\perp, ..., \mathbf{Y}_{n-m}^\perp\}$ provides an instantaneous decomposition of the tangent space. As such, the system's velocities $\dot\gamma(t)$ can be decomposed as

$$\dot\gamma(t) = \sum_{a=1}^{m} w_a(t)\mathbf{Y}_a + \sum_{b=1}^{n-m} s_b(t)\mathbf{Y}_b^\perp, \tag{4}$$

where $w_a(t)$ and $s_b(t)$ are the velocities in the controlled and uncontrolled directions, respectively. Because the basis $\{\mathcal{Y}, \mathcal{Y}^\perp\}$ is normalized with respect to the inertia matrix, the vector fields represent pure directions on the tangent space, and $w_a(t)$ and $s_b(t)$ correspond to the magnitudes of the controlled and uncontrolled velocities. Enforcing orthonormality in Equation (4), it is trivial to solve for the velocities.

The time rate of change of $w_a(t)$ in the $\mathbf{Y}_a$ direction is directly controlled by the inputs. In contrast, the time rate of change of the uncontrolled velocities are independent of the inputs and can only be affected by the control through the coupling of the system's natural dynamics, which can be obtained by computing the time derivative of $s_b(t)$,

$$\begin{aligned}\frac{d}{dt}s_b(t) &= -w_a(t)w_p(t)\mathbf{B}_1^{ap}(\mathbf{Y}_a, \mathbf{Y}_p)\\ &- w_a(t)s_r(t)\mathbf{B}_2^{ar}(\mathbf{Y}_a, \mathbf{Y}_r^\perp) - s_r(t)w_p(t)\mathbf{B}_3^{rp}(\mathbf{Y}_r^\perp, \mathbf{Y}_p)\\ &- s_r(t)s_k(t)\mathbf{B}_4^{rk}(\mathbf{Y}_r^\perp, \mathbf{Y}_k^\perp) - \mathbf{B}_5^b(\mathcal{V}, \mathbf{Y}_b^\perp),\end{aligned} \tag{5}$$

where the repeated indices imply summation. The general forms of the matrices of scalar coefficients are

$$\begin{aligned}\mathbf{B}_1^{ap}(\mathbf{Y}_a, \mathbf{Y}_p) &= \Big(\frac{\partial Y_p^k}{\partial q_i}Y_a^i + \Gamma_{ij}^k Y_a^i Y_p^j\Big)M_{kl}Y_b^{\perp l},\\ \mathbf{B}_2^{ar}(\mathbf{Y}_a, \mathbf{Y}_r^\perp) &= \Big(\frac{\partial Y_r^{\perp k}}{\partial q_i}Y_a^i + \Gamma_{ij}^k Y_a^i Y_r^{\perp j}\Big)M_{kl}Y_b^{\perp l},\\ \mathbf{B}_3^{rp}(\mathbf{Y}_r^\perp, \mathbf{Y}_p) &= \Big(\frac{\partial Y_p^k}{\partial q_i}Y_r^{\perp i} + \Gamma_{ij}^k Y_r^{\perp i} Y_p^j\Big)M_{kl}Y_b^{\perp l},\\ \mathbf{B}_4^{rk}(\mathbf{Y}_r^\perp, \mathbf{Y}_k^\perp) &= \Big(\frac{\partial Y_k^{\perp k}}{\partial q_i}Y_r^{\perp i} + \Gamma_{ij}^k Y_r^{\perp i} Y_k^{\perp j}\Big)M_{kl}Y_b^{\perp l},\\ \mathbf{B}_5^b(\mathcal{V}, \mathbf{Y}_b^\perp) &= \frac{\partial \mathcal{V}}{\partial q_l}Y_b^{\perp l}.\end{aligned} \tag{6}$$

The expression for how $s_b(t)$ changes with time provides an analytical measure of the dynamic coupling between the controlled and uncontrolled velocities. Multiplying a $w^2(t)$ term, the $\mathbf{B}_1$ coefficients quantify how much the controlled velocities can directly affect the rate of change of the uncontrolled velocity. The $\mathbf{B}_2$ and $\mathbf{B}_3$ terms give a measure of the nonlinear coupling between the controlled and uncontrolled velocities since they multiply both $w(t)$ and $s(t)$. The $\mathbf{B}_4$ coefficients multiply an $s^2(t)$ term, so these terms are independent of the control inputs. Similarly, the $\mathbf{B}_5$ term represents the gravity contribution. Hence, the first three terms provide the analytical measure of the dynamic coupling in the system. When evaluated for all configurations along a trajectory, they quantify the system's control authority over the uncontrolled velocities.

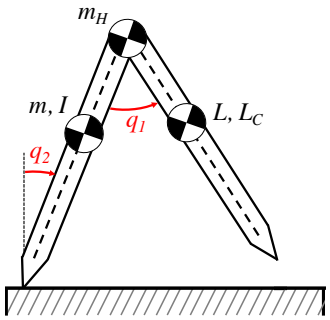


Fig. 1: Two-link biped model. Relative hip angle $q_1$ is actuated; absolute stance angle $q_2$ is unactuated.

### B. Application to Two-Link Biped Model

The two-link planar biped model in Fig. 1 has the geometric and inertial parameters listed in Table I. The rigid-link, point-foot model is left-right symmetric and underactuated during single support, wherein the equations of motion are expressed using generalized coordinates $\mathbf{q} = [q_1, q_2]^T$,

$$\mathbf{M}(\mathbf{q})\ddot{\mathbf{q}} + \mathbf{C}(\mathbf{q}, \dot{\mathbf{q}})\dot{\mathbf{q}} + \mathbf{G}(\mathbf{q}) = \mathbf{B}(\mathbf{q})u, \quad \mathbf{q} \notin \mathcal{S} \tag{7}$$

where $\mathbf{M}(\mathbf{q}) \in \mathbb{R}^{2\times2}$ is the inertia matrix, $\mathbf{C}(\mathbf{q}, \dot{\mathbf{q}}) \in \mathbb{R}^{2\times2}$ is the Coriolis matrix, $\mathbf{G}(\mathbf{q}) \in \mathbb{R}^2$ is the gravity vector, $\mathbf{B}(\mathbf{q}) \in \mathbb{R}^{2\times1}$ is the actuation matrix mapping actuator torques to joint torques, and $u \in \mathbb{R}$ is the control input.

The hypersurface $\mathcal{S}$ is a switching set that defines the limits of the continuous dynamics and relates the generalized coordinates $\mathbf{q}^-$ immediately before impact to the state $\mathbf{q}^+$ immediately after impact via the discrete map,

$$\begin{aligned}\mathbf{q}^+ &= \mathbf{\Delta}_{\mathbf{q}}\mathbf{q}^-, \quad &\mathbf{q} \in \mathcal{S},\\ \dot{\mathbf{q}}^+ &= \mathbf{\Delta}_{\dot{\mathbf{q}}}\dot{\mathbf{q}}^-, \quad &\mathbf{q} \in \mathcal{S},\end{aligned} \tag{8}$$

where $\mathbf{\Delta}_{\mathbf{q}}$ is the $n\times n$ switching matrix and $\mathbf{\Delta}_{\dot{\mathbf{q}}}$ is an $n \times n$ matrix relating pre- and post-impact velocities. If $\mathbf{x} = [\mathbf{q}^T, \dot{\mathbf{q}}^T]^T$, Equations (7)-(8) may be written in state-space form using coupled first-order differential equations.

$$\Sigma : \begin{cases}\dot{\mathbf{x}} = \mathbf{f}(\mathbf{x}, u), & \mathbf{x} \notin \mathcal{S},\\ \mathbf{x}^+ = \mathbf{\Delta}(\mathbf{x}^-), & \mathbf{x} \in \mathcal{S}.\end{cases} \tag{9}$$

TABLE I: Parameters of two-link biped model. Center of mass (CoM) location is measured from hip. Mass moment of inertia is measured about segment's CoM.

| Symbol | Parameter Description | Units | Value |
|---|---|---|---|
| $L$ | Leg length | m | 1.0 |
| $L_C$ | Leg CoM | m | 0.5 |
| $m$ | Leg mass | kg | 3.0 |
| $m_H$ | Hip mass | kg | 10.0 |
| $I$ | Leg inertia | kg·m$^2$ | 0.02 |

Because the biped is actuated at the hip only, the input torque can be defined by $\mathbf{F}^1 = u\,[1,0]^T$. In this case, there is only one controlled direction $\mathbf{Y}_1$ and one uncontrolled direction $\mathbf{Y}_1^\perp$, so the subscripts indexing the directions are dropped. The system velocities can be decomposed in terms of the input vector field and its orthogonal complement, $\dot{\boldsymbol{\gamma}}(t) = w(t)\mathbf{Y} + s(t)\mathbf{Y}^\perp$. Taking the time derivative of $s(t)$, $\mathbf{B}_3$ is the only non-zero coupling coefficient for this model. Consequently, the rate of change of $s(t)$ simplifies to

$$\frac{d}{dt}s(t) = -s(t)w(t)\mathbf{B}_3(\mathbf{Y}^\perp, \mathbf{Y}) - \mathbf{B}_5(\mathcal{V}, \mathbf{Y}^\perp). \tag{10}$$

The single coupling coefficient motivates use of the two-link biped model as an exploratory example.

While the degree to which the controlled and uncontrolled directions are coupled is a function of the configuration and system parameters only, the coupling itself is proportional to the velocities, so a non-zero velocity is necessary for there to be any coupling, hence the term "dynamic coupling." As such, in the remainder of this paper, the bilinear term $s(t)w(t)\mathbf{B}_3(\mathbf{Y}^\perp, \mathbf{Y})$, which has units of $m^2\sqrt{kg}/s^2$, will be referred to as the *coupling*. The bilinear term is considered rather than just the coefficient because nonzero velocities more closely mimic those of useful bipedal gaits.

## III. Gait Optimization

The trajectory optimization problem to minimize the cost function $\mathcal{J}(\mathbf{x}, u)$ can be formulated as

$$\begin{aligned} \underset{\mathbf{x}^\star, u^\star}{\text{argmin}} \quad & \mathcal{J}(\mathbf{x}, u) \\ \text{s.t.} \quad & \dot{\mathbf{x}} = \mathbf{f}(\mathbf{x}, u), \\ & \mathbf{c}_{\text{min}} \leq \mathbf{c}(\mathbf{x}, u) \leq \mathbf{c}_{\text{max}}, \\ & \mathbf{b}_{\text{min}} \leq \mathbf{b}(\mathbf{x}^+, \mathbf{x}^-) \leq \mathbf{b}_{\text{max}}, \end{aligned} \tag{11}$$

where $\mathbf{f}(\mathbf{x}, u)$ denotes the system dynamics during single support, $\mathbf{c}(\mathbf{x}, u)$ is a collection of constraints, and $\mathbf{b}(\mathbf{x}^+, \mathbf{x}^-)$ represents the boundary conditions, including the discrete impact map for gait periodicity. Solutions are feasible motions — states and control inputs that satisfy all constraints.

Gait optimization problems are typically solved via shooting methods or transcription methods [11]. Shooting methods integrate the full system dynamics by *shooting* trajectories from starting points. This paper uses direct transcription, in which the trajectory is parameterized by discrete collocation points that include the states and control inputs [12]. The equations of motion are satisfied at the collocation points. Both shooting and transcription methods create a nonlinear programming problem to be solved by state-of-the-art solvers, such as *IPOPT* [13]. In this work, 30 finite elements were chosen to discretize the trajectory, and the states and control inputs within each segment were approximated with 3rd-order Lagrange polynomials.

Table II lists the constraints enforced in the optimization to generate realistic gaits, including actuator limits of 15 N·m, a conservative slew rate of 0.01 second for the torque's rate of change, a coefficient of static friction of 0.6. When the normal ground reaction force (GRF) $F_n$ gets close to 0, the friction cone constraint $|F_t| \leq \mu_s F_n$ becomes harder to satisfy, a situation that may arise early and late in the gait cycle. Thus, the minimum normal GRF was set to 20 N ($1/8$ of its maximum value in the quasi-static case), which is a technique that has proven effective in experiment [14]. To achieve more consistent foot touchdown, the magnitude of the swing foot horizontal velocity was constrained to be less than 0.10 m/s in the last 10% of the gait cycle.

TABLE II: Optimization constraints & parameters

| Constraint Description | Value |
|---|---|
| $\mathbf{q}$ (rad) | $-\pi/3 \leq q_1, q_2 \leq \pi/3$ |
| $\dot{\mathbf{q}}$ (rad/s) | $\dot{q}_2 > 0$ |
| $\mathbf{u}$ (N·m) | $\lvert u\rvert \leq 15$ |
| Slew rate (s) | $t_{slew} = 0.01$ |
| Step length, D (m) | $0.30 \leq D \leq 0.95$ |
| Step duration, T (s) | $0.50 \leq T \leq 1.20$ |
| Static friction coefficient | $\mu_s = 0.6$ |
| Minimum vertical GRF (N) | $F_n \geq 20$ |

The specific energetic cost of transport (SCOT), a dimensionless measure of the energy required to move one kilogram one meter [15], was used as the cost function to optimize gaits for energetic efficiency.

$$\mathcal{J}_{SCOT} = \frac{1}{M\,g\,D}\int_0^T |u(t)\dot{q}_1(t)|\,dt, \tag{12}$$

where the integral represents the work done by the actuator over a step, $T$ is the step period, $D$ is the step length, and $M$ is the biped's total mass. A total of 5450 periodic gaits that minimized $\mathcal{J}_{SCOT}$ were generated using an evenly-spaced grid search to span walking speeds from 0.50 m/s to 1.00 m/s and step lengths from 0.30 m to 0.95 m, with step period constrained to be between 0.50 and 1.20 s.

## IV. Simulation Studies

### A. Feedback Control

Collocation introduces discretization errors since feasibility is guaranteed only at the collocation points. Therefore, the open-loop gait trajectories must be feedback-stabilized, and hybrid zero dynamics (HZD)-based control is the low-level controller in this work [16]. HZD-based control defines the desired trajectories of the actuated DoF as holonomic constraints and employs feedback linearization and high-gain PD control to drive those constraints to zero [17].

With a single actuated DoF,

$$y = h(\mathbf{q}) = q_1 - q_1^\star(q_2) \tag{13}$$

is the lone holonomic constraint, where $q_1^\star(q_2)$ encodes the desired configuration as a function of step progression. Feedback linearization achieves a new input/output linear system, and the output equation must be differentiated twice before the control input $u$ appears explicitly.

$$\ddot{y} = L_f^2 h + L_g L_f h\, u, \tag{14}$$

where $L_f h$ represents the Lie derivative of $h$ with respect to $\mathbf{f}$ [18]. Hence, the system has relative degree two, and the input of the new system is

$$u = (L_g L_f h)^{-1}(\mathrm{v} - L_f^2 h), \tag{15}$$

where $\mathrm{v} = \ddot{y}$. High-gain PD feedback guarantees exponential convergence to the target trajectory.

$$\mathrm{v} = K_P y + K_D \dot{y}. \tag{16}$$

The gaits were simulated using MATLAB's `ode45`, and $K_P = 500$ and $K_D = 10$ stabilized the gaits to their respective nominal trajectories.

### B. Correlation Between Coupling and Robustness

The quantitative measure of gait robustness should characterize the ability to remain stable in the presence of external disturbances or modelling errors. The gait's region of attraction (RoA) — the set of all states for which the walker converges to the nominal periodic orbit — has proven to be an effective measure of gait robustness [19]. Estimating the gait's RoA, however, involves simulating Eq. (9) forward in time starting at all possible initial conditions, so it becomes intractable as more DoF are added. For instance, estimating the RoA of the two-link biped requires discretization and simulation of a 4D space, which motivates a simpler alternative. Simulation and experimental studies on underactuated walkers have suggested that observing the behavior of the unactuated DoF alone is sufficient to predict falls [20]. The RoA of the unactuated dynamics can be defined as the reduced space in which a biped can be guaranteed to walk forever, and this reduced RoA captures the main failure modes of underactuated dynamics walkers [21].

The reduced RoA of each gait was estimated numerically by discretizing the unactuated dynamics $(q_2; \dot{q}_2)$ using 100 evenly-spaced intervals for $q_2$ and an adjustable step-size search in $\dot{q}_2$. Each initial condition $\mathbf{x_0} := \left(q_1^\star(q_2); q_2; \dot{q}_1^\star(q_2); \dot{q}_2\right)$ was simulated using MATLAB's `ode45` with default options, where the actuated states took on their steady-state values, hence the $^\star$ notation. Each $\mathbf{x_0}$ was added to the RoA if it satisfied $\lim_{t\to\infty} dist\big(\varphi(t, \mathbf{x_0}), (q_2^\star, \dot{q}_2^\star)\big) = 0$, where $\varphi(t, \mathbf{x_0})$ represents the realization of the dynamical system. More details can be found in [22], Section IV.

Pearson's correlation coefficient quantifies the relationship between the instantaneous coupling and the tighest bound on the RoA throughout the gait. For data sets $X$ and $Y$, Pearson's correlation coefficient returns a value between $-1$ and 1,

$$\rho_{X,Y} = \frac{\mathrm{cov}(X, Y)}{\sigma_X \sigma_Y}, \tag{17}$$

where $\mathrm{cov}(\cdot)$ denotes the covariance and $\sigma_{(\cdot)}$ is the standard deviation. The resulting correlation coefficient for each gait is plotted in Fig. 2, which shows that the correlation increased with walking speed and decreased with step length. More importantly, every gait showed a positive correlation coefficient greater than 0.38, suggesting **positive correlation between coupling and robustness**. The mean correlation value was 0.70, and most gaits were in the range of 0.6 to 0.93, suggesting strong correlation ($\rho \approx 0$ indicating no correlation). This finding is intuitive: *strong coupling is needed to have good disturbance rejection performance*. Similar correlation results were found when the same grid of gaits was generated by minimizing the integral of torque-squared over a step instead of SCOT.

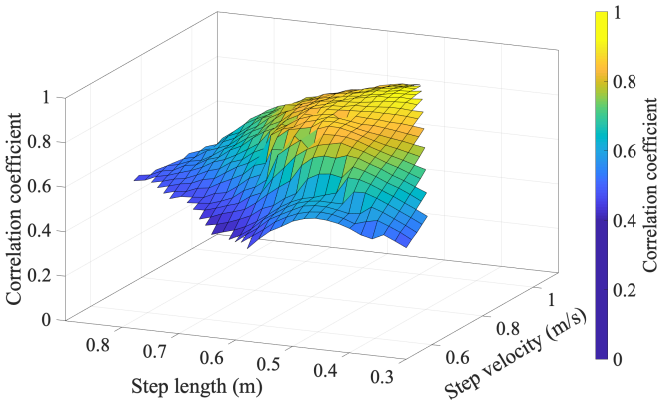


Fig. 2: Pearson's correlation coefficient between coupling and robustness for 5450 gaits minimizing SCOT ($\bar{\rho} = 0.701$). Warmer colors indicate stronger correlation. Coefficients statistically significant at 99% confidence level ($p < 0.01$).

### C. Robustness of Coupling-Optimized Gaits

While the results in Fig. 2 do not necessarily imply causality between coupling and robustness, the correlation motivated exploration of two-link gaits designed to maximize/minimize coupling strength as quantified by the integral of the coupling over a step,

$$\mathcal{J}_{coup} = \int_0^T s(t) w(t) \mathbf{B}_3(\mathbf{Y}^\perp, \mathbf{Y})\, dt. \tag{18}$$

In this case, only the desired walking speed was constrained to be 0.75 m/s, the mid-point of the range considered in Section III, while the step length and step period were determined by the optimizer to explore the effect of increased/decreased coupling on step characteristics. The gaits minimizing SCOT and maximizing coupling had similar step lengths and periods, whereas the gait minimizing coupling had a longer step length and period. The step characteristics for the generated gaits are listed in Table III, and the video attachment provides side-by-side gait animations.

TABLE III: Step characteristics of 0.75 m/s gaits.

| Objective | Step Length (m) | Step Period (s) |
|---|---|---|
| SCOT | 0.595 | 0.793 |
| Maximized Coupling | 0.544 | 0.725 |
| Minimized Coupling | 0.869 | 1.159 |

Gait stability was assessed using the method of Poincaré, with the nonlinear system reduced to a discrete representation mapping the states at a particular instant of the gait cycle from one step to the next $\mathbf{x}_{k+1} = \mathbf{P}(\mathbf{x}_k)$. The linearization of $\mathbf{P}(\cdot)$ about its fixed point determines exponential stability of the limit cycle, where the fixed point is the intersection of the nominal limit cycle and the Poincaré section. The linearized system

$$\delta\mathbf{x}_{k+1} = \mathbf{A}\delta\mathbf{x}_k, \tag{19}$$

where $\delta\mathbf{x}_k = \mathbf{x}_k - \mathbf{x}^\star$ and $\mathbf{A}$ is the Jacobian of the Poincaré map, can be found by perturbing the walker in simulation. The eigenvalues of $\mathbf{A}$, sometimes referred to as the Floquet multipliers, must all be inside the unit circle for the gait to be stable. For this work, a disturbance of $-0.001$ (rad or rad/s) was applied to each DoF consecutively, and the largest Floquet multiplier of every gait had magnitude smaller than one, suggesting that all gaits were stable. While in theory indicating how rapidly the walker should converge to its limit cycle, the largest Floquet multiplier is known to be a poor indicator of a gait's disturbance rejection performance [19]. As such, it is only used herein to infer gait stability.

Gait robustness was instead first evaluated by stochastic performance on uneven terrain. Changes in terrain height at every step were randomly drawn from a normal Gaussian distribution $\mathcal{N}(\mu, \sigma)$, where the standard deviation $\sigma$ represents the terrain noise level and was kept low (<1% of leg length) since the two-link model has weak disturbance rejection capabilities. Two hundred such terrains, each consisting of 5,000 steps, were generated for noise levels with mean value $\mu = 0$. For noise levels below $\sigma = 0.06$ cm, the robot successfully traversed every terrain regardless of gait. For higher noise levels, however, the robot was guaranteed to fall with probability 1 as $t \to \infty$, so the average number of steps before failure quantifies stochastic performance. This metric is akin to the more popular mean of first passage time [23], but is easier to compute in simulation and more practical to observe in experiment.

All four gaits were evaluated over the 200 terrain profiles

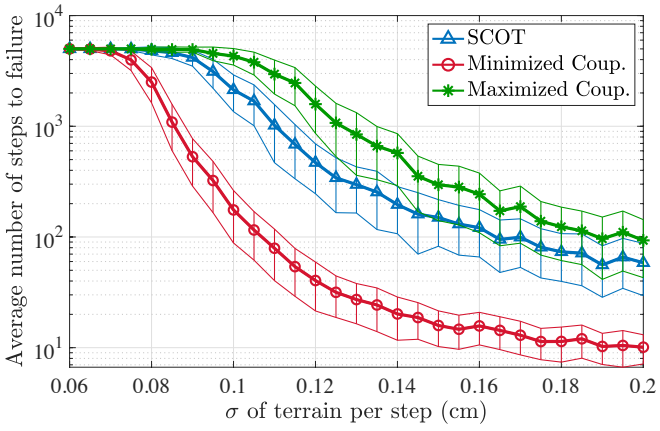


Fig. 3: Stochastic performance of 0.75-m/s gaits. Error bars indicate $\pm$ 1 standard deviation.

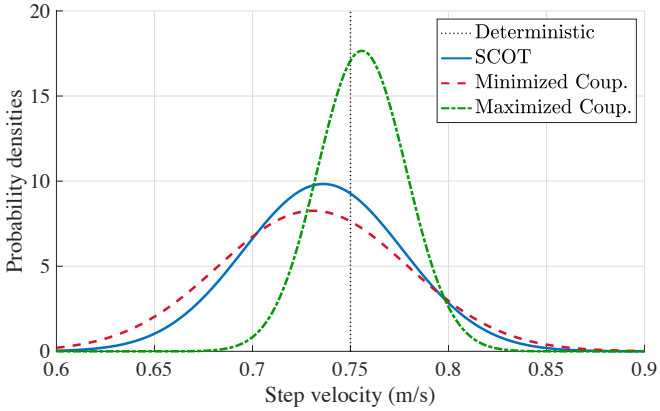


Fig. 4: Step velocity probability density function of 250 steps for $\sigma = 0.06$ cm. Design walking speed is 0.75 m/s.

for each noise level. Figure 3 summarizes the results of each trial, which started with the biped at steady state and ended after completing 5,000 steps or falling down. The SCOT-minimizing gait showed increased robustness in comparison to the gait minimizing coupling, but the gait maximizing coupling had better stochastic performance as expected.

Next, the gaits' ability to maintain a desired walking speed on stochastic terrain was assessed using the step velocity probability density function (PDF) of 250 steps when $\sigma =$ 0.06 cm. As seen in Fig. 3, this level of noise permitted each gait to traverse the full terrain at every trial. The robot again started each simulation at steady state, and kinematic data for all 250 steps were recorded. The step velocity PDF for each gait is plotted in Fig. 4, showing that the gait maximizing coupling better maintained desired walking speed than the other gaits. This is not surprising since the superior stochastic performance of the gait maximizing coupling would suggest stronger attraction to the fixed point. The gait maximizing coupling pulls the system dynamics toward its limit cycle more effectively when they wander inside the RoA. Table IV summarizes the results and lists the mean SCOT for each gait. As expected, the gait minimizing SCOT had the lowest SCOT; that of the gait maximizing coupling was nearly 4 times higher. While this suggests that the enhanced robustness came at the expense of energetic efficiency, a SCOT of 0.05 remains quite low, even in the realm of underactuated walkers. The gait minimizing coupling returned a SCOT nearly an order of magnitude higher than the optimal efficiency gait, which suggests that minimizing coupling has a more adverse effect on energetic efficiency than does maximizing coupling.

TABLE IV: Average step velocity and specific energetic cost of transport (SCOT) when $\sigma = 0.06$ cm ($\pm$ std dev).

| Objective | Step Velocity (m/s) | SCOT |
|---|---|---|
| SCOT | 0.736±0.041 | 0.013±0.002 |
| Maximized Coupling | 0.756±0.023 | 0.052±0.005 |
| Minimized Coupling | 0.731±0.048 | 0.109±0.007 |

TABLE V: Change in size of region of attraction (RoA) with respect to SCOT-minimizing gait. "+" and "−" indicate enlarged and shrunk RoA, respectively. First column indicates timing of disturbance. $q_2^+$ and $q_2^-$ denote instants before and after impact (0% and 100%).

| | | Change in RoA Size | |
|---|---|---|---|
| Gait cycle | RoA (rad/s) | Maximized Coupling | Minimized Coupling |
| $q_2^+$ | −0.078 | +15% | −61% |
| 20% | −0.126 | +6% | −50% |
| 40% | −0.306 | +10% | −54% |
| 60% | −0.183 | +6% | −62% |
| 80% | −0.117 | +12% | −57% |
| $q_2^-$ | −0.083 | +14% | −58% |

Using the method from Section IV.B, each gait's RoA at the instant right after ground impact ($q_2^+$) is plotted as a contour map in Fig. 5, where the origin represents the fixed point itself and $\delta q_2$ and $\delta \dot{q}_2$ indicate how far from the nominal limit cycle the robot can deviate without falling. This map shows that the RoA of the gait maximizing coupling is the largest and that the gaits are more sensitive to deceleration disturbances (tighter bounds on RoA when $\delta \dot{q}_2 < 0$). The results for the full gait cycle are summarized in Table V, where the 3rd and 4th columns report the change in RoA size as a percentage of the RoA of the SCOT-optimized gait (2nd column). As expected, maximizing/minimizing the coupling strength during gait design enlarged/shrunk the RoA throughout the full gait cycle.

Finally, the gaits were assessed in terms of robustness to model uncertainties, a critical aspect of gait design since modeling errors always exist in practice. Model uncertainties were simulated by adding/removing mass at the hip by up to 30% (nominally 10 kg). Figure 6 shows gait robustness as measured by the difference between the desired and actual walking speeds after convergence to steady state. While the gait minimizing coupling performed well for a small range of mass variations (−8% to 0%), the gait maximizing coupling was more robust to model uncertainties. Nearly identical performance was achieved across the same range of disturbances when optimizing for the integral of torque-squared over a step rather than SCOT.

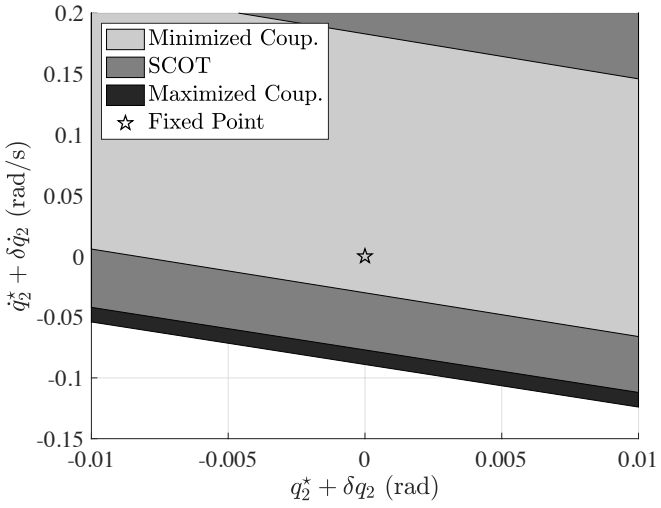


Fig. 5: Snapshot of unactuated dynamics RoA after impact.

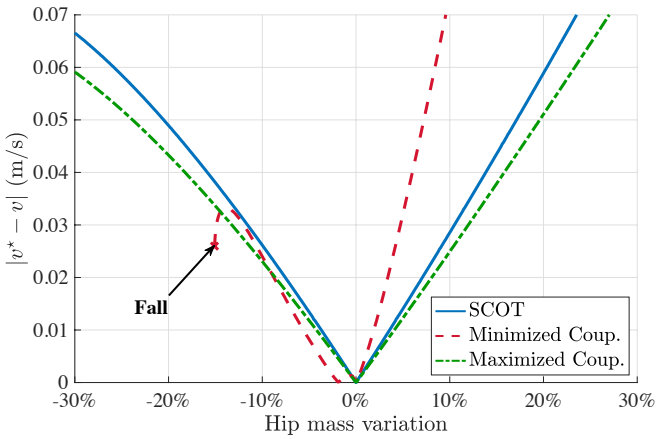


Fig. 6: Deviation from nominal walking speed under model uncertainty introduced by adding/removing mass at the hip.

## V. Conclusions

This paper analyzed the effect of dynamic coupling on overall gait robustness for an underactuated two-link biped model. The velocity decomposition framework provides an analytical measure of the coupling that was used in the context of trajectory optimization. The main contribution is the finding that the increased coupling between the controlled and uncontrolled directions is strongly correlated to the enhanced robustness of the two-link gaits. To further demonstrate dynamic coupling's practical implications for gait design, this paper compared the robustness of gaits minimizing and maximizing coupling. Robustness was assessed using:

1) stochastic performance on uneven terrain as quantified by the average number of steps taken before falling,
2) ability to maintain the desired walking speed under non-vanishing disturbances,
3) size of the region of attraction (RoA),
4) robustness to model uncertainties.

In all 4 cases, robustness of the gait maximizing coupling was superior to that of the gait minimizing coupling.

The formulation is general in that it applies to any underactuated mechanical system whose dynamics can be described by Lagrange's equations. Thus, future work aims to extend this analysis to more complex bipeds with more coupling terms and validate the findings in experiment. A promising avenue for gait optimization is exploiting the instantaneous nature of the coupling metric. When the robot can anticipate a disturbance, it is possible to employ a gait that momentarily puts the biped in a position with strong coupling.

## REFERENCES


[1] T. McGeer, "Passive walking with knees," in *Proc. IEEE Int. Conf. Robotics and Automation*, 1990, pp. 1640–1645.

[2] P. A. Bhounsule, J. Cortell, A. Grewal, B. Hendriksen, J. G. D. Karssen, C. Paul, and A. Ruina, "Low-bandwidth reflex-based control for lower power walking: 65 km on a single battery charge," *Int. J. Robotics Research*, vol. 33, no. 10, pp. 1305–1321, 2014.

[3] F. Bullo and A. D. Lewis, *Geometric control of mechanical systems: modeling, analysis, and design for simple mechanical control systems*. Springer Science & Business Media, 2004, vol. 49.

[4] J. Nightingale, R. Hind, and B. Goodwine, "Intrinsic vector-valued symmetric form for simple mechanical control systems in the nonzero velocity setting," in *Proc. IEEE Int. Conf. Robotics and Automation*, 2008, pp. 2435–2440.

[5] M. Fevre, B. Goodwine, and J. P. Schmiedeler, "Design and experimental validation of a velocity decomposition-based controller for underactuated planar bipeds," *IEEE Robotics & Automation Letters*, vol. 3, no. 3, pp. 1896–1903, 2018.

[6] M. Fevre, B. Goodwine, and J. P. Schmiedeler, "Terrain-blind walking of planar underactuated bipeds via velocity decomposition-enhanced control," *Int. J. Robotics Research*, vol. 38, no. 10–11, pp. 1307–1323, 2019.

[7] B. Goodwine and J. Nightingale, "The effect of dynamic singularities on robotic control and design," in *Proc. IEEE Int. Conf. Robotics and Automation*, 2010, pp. 5213–5218.

[8] D. C. Post, B. Goodwine, and J. P. Schmiedeler, "Quantifying control authority in periodic motions of underactuated mobile robots," in *Proc. ASME Int. Des. Eng. Technical Conf. and Computers and Inf. in Eng. Conf.*, 2015, p. V05AT08A061.

[9] T. Chen, X. Ni, J. P. Schmiedeler, and B. Goodwine, "Using a nonlinear mechanical control coupling metric for biped robot control and design," in *Proc. IEEE Int. Conf. on Methods and Models in Automation and Robotics*, 2017, pp. 903–908.

[10] J. Nightingale, R. Hind, and B. Goodwine, "A stopping algorithm for mechanical systems," in *Algorithmic Foundation of Robotics VIII*. Springer, 2009, pp. 167–180.

[11] M. Kelly, "An introduction to trajectory optimization: how to do your own direct collocation," *SIAM Review*, vol. 59, no. 4, pp. 849–904, 2017.

[12] J. T. Betts, "Survey of numerical methods for trajectory optimization," *J. Guidance, Control, and Dynamics*, vol. 21, no. 2, pp. 193–207, 1998.

[13] C. Laird and A. Wächter, "Introduction to IPOPT: a tutorial for downloading, installing, and using IPOPT," 2006.

[14] B. Griffin and J. Grizzle, "Nonholonomic virtual constraints and gait optimization for robust walking control," *The International Journal of Robotics Research*, vol. 36, no. 8, pp. 895–922, 2017.

[15] S. Collins, A. Ruina, R. Tedrake, and M. Wisse, "Efficient bipedal robots based on passive-dynamic walkers," *Science*, vol. 307, no. 5712, pp. 1082–1085, 2005.

[16] E. R. Westervelt, J. W. Grizzle, C. Chevallereau, J. H. Choi, and B. Morris, *Feedback Control of Dynamic Bipedal Robot Locomotion*. CRC Press, 2007.

[17] E. R. Westervelt, J. W. Grizzle, and D. E. Koditschek, "Hybrid zero dynamics of planar biped walkers," *IEEE Trans. Autom. Control*, vol. 48, no. 1, pp. 42–56, 2003.

[18] A. Isidori, *Nonlinear Control Systems*. Springer Science & Business Media, 2013.

[19] D. G. Hobbelen and M. Wisse, "A disturbance rejection measure for limit cycle walkers: The gait sensitivity norm," *IEEE Transactions on robotics*, vol. 23, no. 6, pp. 1213–1224, 2007.

[20] M. Fevre, H. Lin, and J. P. Schmiedeler, "Stability and gait switching of underactuated biped walkers," in *Proc. IEEE/RSJ Int. Conf. Intelligent Robots and Systems*, 2019, pp. 2279–2285.

[21] C. O. Saglam and K. Byl, "Stability and gait transition of the five-link biped on stochastically rough terrain using a discrete set of sliding mode controllers," in *Proc. IEEE Int. Conf. Robotics and Automation*, 2013, pp. 5675–5682.

[22] M. Fevre, B. Goodwine, and J. Schmiedeler, "Velocity decomposition-enhanced control for point and curved-foot planar bipeds experiencing velocity disturbances," *ASME J. Mechanisms and Robotics*, vol. 11, no. 2, 2019.

[23] K. Byl and R. Tedrake, "Metastable walking machines," *Int. J. Robotics Research*, vol. 28, no. 8, pp. 1040–1064, 2009.